# Effects of the surface conductivity and the IMF strength on the dynamics of planetary ions in Mercury's magnetosphere

Kanako Seki, Naoki Terada, Manabu Yagi, Dominique C. Delcourt, François Leblanc, Tatsuki Ogino

JOURNAL OF GEOPHYSICAL RESEARCH: SPACE PHYSICS, VOL. 118, 3233–3242, doi:10.1002/jgra.50181, 2013

# Effects of the surface conductivity and the IMF strength on the dynamics of planetary ions in Mercury's magnetosphere

K. Seki,[1] N. Terada,[2] M. Yagi,[2] D. C. Delcourt,[3] F. Leblanc,[4] and T. Ogino[1]

Received 1 November 2012; revised 23 January 2013; accepted 10 February 2013; published 21 June 2013.

[1] To examine the effects of planetary surface conductivity and the southward interplanetary magnetic field (IMF) strength on ion dynamics, systematic trajectory tracings of $Na^+$ ions were performed in the electric and magnetic field configurations obtained from magnetohydrodynamics (MHD) simulations of the solar wind-Mercury interaction. Comparison with a previous study, which used an analytical model that rescaled the Earth's magnetosphere and assumed the existence of the distant neutral line (DNL) in Mercury's magnetotail, shows a drastic change in the $Na^+$ precipitation pattern due to the formation of the near-Mercury neutral line (NMNL) in MHD simulations. The $Na^+$ precipitation band at approximately 30° of latitude (LAT), which was obtained in the previous study, disappeared in the equivalent low-conductivity MHD case due to the NMNL formation, while the NMNL formation causes high-energy $Na^+$ precipitation in the equatorial region. The change in strength of the southward IMF (sBz) alters the location of the NMNL and the $Na^+$ precipitation pattern. In the low-conductivity sBz = 5 case, both the equatorial precipitation and the $Na^+$ band at approximately LAT = 30 are formed. In the high-conductivity sBz = 5 case, magnetospheric convection through the polar regions is suppressed, which results in a region of dense $Na^+$ near the planet. These results suggest that the precipitation pattern of planetary ions onto Mercury's surface changes significantly with the activity level of Mercury's magnetosphere. It is also suggested that observations of the magnetospheric convection, the distribution of $Na^+$ ions around the planet, or the precipitation pattern of $Na^+$ ions onto the planetary surface can provide us information about the surface conductivity.

**Citation:** Seki, K., N. Terada, M. Yagi, D. C. Delcourt, F. Leblanc, and T. Ogino (2013), Effects of the surface conductivity and the IMF strength on the dynamics of planetary ions in Mercury's magnetosphere, *J. Geophys. Res. Space Physics*, *118*, 3233–3242, doi:10.1002/jgra.50181.

## 1. Introduction

[2] Observations by Mariner-10 in the 1970s revealed the existence of an intrinsic magnetic field of Mercury [*Ness et al.*, 1975], and it has been confirmed and revised by recent MESSENGER observations [*Anderson et al.*, 2008, 2011] with a reduced (∼1/2800) dipole moment compared to that of the Earth. The spatial and temporal scales of the resulting magnetosphere are expected to be much smaller than those of the Earth's magnetosphere. During MESSENGER's first Mercury flyby, various planetary heavy ion species such as $Na^+$, $O^+$, $Mg^+$, $K^+$, $Ca^+$, $S^+$, and $H_2S^+$ were observed; in particular, $Na^+$ and $O^+$ fill the wide region of the magnetosphere [*Zurbuchen et al.*, 2008]. The interplanetary magnetic field (IMF) was northward during the flyby, and a quiet magnetosphere with double current sheet at the dawnside magnetopause was observed [*Slavin et al.*, 2008] in contrast to the magnetotail observation by Mariner-10, which showed high-energy (> several tens of keVs) electron injections in conjunction with a rapid change of the magnetic field orientation [e.g., *Ogilvie et al.*, 1977]. Recent MESSENGER observations showed that the polar regions were important sources of planetary heavy ions such as $Na^+$ and $O^+$ in Mercury's magnetosphere through solar-wind sputtering near the poles [*Zurbuchen et al.*, 2011]. However, the mechanism responsible for particle acceleration in the small magnetosphere remains controversial [e.g., *Siscoe et al.*, 1975; *Luhmann et al.*, 1998]. To further examine the issue, one needs to understand the basic structure and dynamics of Mercury's magnetosphere, including the global convection pattern and the plasma supply processes in Mercury's magnetosphere. This goal has motivated several numerical studies using

[1]Solar-Terrestrial Environment Laboratory, Nagoya University, Nagoya, Aichi1, Japan.
[2]Department of Geophysics, Tohoku University, Sendai, Miyagi, Japan.
[3]Laboratoire de Physique des Plasmas, Ecole Polytechnique-CNRS-UPMC, Saint Maur des Fosses, France.
[4]LATMOS/IPSL, CNRS, Universite Pierre et Marie Curie, Paris, France.

Corresponding author: K. Seki, Solar-Terrestrial Environment Laboratory, Nagoya University, Furo-cho, Chikusa-ku, Nagoya, Aichi 464-8601, Japan. (seki@stelab.nagoya-u.ac.jp)


2169-9380/13/10.1002/jgra.50181

a variety of modeling approaches (MHD, single-particle, and hybrid) [e.g., *Kabin and Gombosi*, 2000; *Delcourt et al.*, 2003, 2005, 2012; *Delcourt and Seki*, 2006; *Kallio and Janhunen*, 2004; *Janhunen and Kallio*, 2004].

[3] In order to understand the global configuration of Mercury's magnetosphere, there are two important boundary conditions: the solar wind conditions and the planetary surface conductivity. Comparison between observations by Mariner-10 and those by MESSENGER suggests that the north-south component of IMF can play an important role in the activity level of the magnetosphere as discussed above [e.g., *Slavin et al.*, 2008, 2010]. Meanwhile, *Kallio and Janhunen* [2004] reported that the difference between the northward and the southward IMF cases are not drastic in their hybrid simulation results, and the IMF effects are not fully understood. On the basis of the hybrid simulations with six cases of surface conductivity models, *Janhunen and Kallio* [2004] also showed the possibility that the surface conductivity could affect the magnetospheric current closure, which may change the magnetospheric configuration.

[4] Another interesting feature of Mercury's magnetosphere is the kinetic effects of heavy planetary ions such as $Na^+$, which have larger Larmor radii than solar wind protons. The tenuous atmosphere of Mercury has been discovered through both ground-based and satellite observations: Mercury's exosphere is known to contain H, He, and O from the Mariner 10 UV observations [e.g., *Broadfoot et al.*, 1976], and sodium (Na), potassium (K), and calcium (Ca) were discovered using ground-based observations [*Potter and Morgan*, 1985, 1986; *Bida et al.* 2000]. Among these planetary species, the Na exosphere is the best investigated, and the existence of the Na tail and its temporal variation has been reported [e.g., *Kameda et al.*, 2007; *McClintock et al.*, 2008]. The Na exosphere is considered to be formed with Na atoms released from the planetary surface. To model the Na exosphere, release processes such as thermal desorption, photon-stimulated desorption, solar wind sputtering, and micro-meteoroid vaporization have been considered [e.g., *Leblanc and Johnson*, 2003; *Mura et al.*, 2007].

[5] The effects of planetary ions on the magnetosphere have been studied based on numerical simulations. Recent multi-component MHD simulation showed that the heavy mass loading due to planetary ions, during the northward IMF period with relatively slow convection, might facilitate the absolutely unstable Kelvin-Helmholtz instability [*Fujimoto et al.*, 2007] . The simulation also suggested that the heavy mass loading might explain the vortex feature observed during the MESSENGER's first flyby [*Slavin et al.*, 2009]. *Delcourt et al.* [2003] conducted systematic trajectory tracings of test $Na^+$ ions in a rescaled analytical model of magnetic and electric fields of the Earth's magnetosphere for Mercury, which used a simplified model of the exosphere with respect to *Leblanc and Johnson* [2003]. The results of the trajectory tracings showed that the non-adiabatic motion of ions in the magnetotail could produce energetic $Na^+$ ions in the magnetosphere and cause a narrow band of energetic (several keV) $Na^+$ precipitation in each hemisphere [*Delcourt et al.*, 2003]. Because these precipitation bands extend over several degrees in latitude and a wide range of longitude, it may lead to additional sputtering of planetary material at the surface. However, it is not evident that the magnetospheric configuration and the global convection pattern in Mercury's magnetosphere can be described using the rescaled geomagnetospheric model. *Sarantos et al.* [2009] conducted the trajectory tracings of $Na^+$ ions in the MHD fields obtained under the northward IMF condition similar to that held during the MESSENGER's first Mercury flyby. Their results showed that the $Na^+$ pick-up process in the solar wind and magnetosheath regions was potentially important in explaining the high-energy $Na^+$ component in the magnetosphere. *Yagi et al.* [2010] also showed the importance of the $Na^+$ pick-up process in the magnetosheath for the formation of the "sodium ring current" around the planet in steady solar wind conditions under the northward IMF.

[6] In this study, we conducted systematic trajectory tracings of test $Na^+$ ions in the electric and magnetic fields obtained from three cases of MHD simulations of the solar wind-Mercury interaction. We focused on the effects of the surface conductivity and the southward IMF strength on the dynamics of planetary ions in Mercury's magnetosphere. The results were compared with those from *Delcourt et al.* [2003], which were obtained for the rescaled analytical model to investigate how the ion dynamics and the resultant $Na^+$ precipitation pattern onto the planetary surface differs from or resemble those in the simple two-cell convection pattern described by the analytical model. It is observationally known that during the southward IMF periods, the Mercury's magnetosphere becomes active, and interesting phenomena such as plasmoids in the magnetotail have been observed by the MESSENGER spacecraft [*Slavin et al.*, 2012]. To understand the effects of the NMNL (near-Mercury neutral line) formation in the active Mercury's magnetosphere, in this study, we focused on the southward IMF cases to compare with the previous study using an analytical model that assumes the southward IMF [*Delcourt et al.*, 2003]. Recent MESSENGER observations showed a significant amount of $O^+$ ions in Mercury's magnetosphere [*Zurbuchen et al.*, 2011]. In this study, we used $Na^+$ ions as an exemplary ion species to study the dynamics of heavy ions in Mercury's magnetosphere. In Section 2, we described the three cases of the global MHD simulation of Mercury's magnetosphere that we used in this study. In Section 3, results of the systematic trajectory tracings are shown. In Section 4, after summarizing the obtained results, we discussed the effects of the southward IMF strength and the surface conductivity on the dynamics of Mercury's magnetosphere by comparing with the case of the analytical model.

## 2. Global MHD Simulation of Mercury'S Magnetosphere

### 2.1. Global MHD Model

[7] To simulate the interaction between the solar wind and Mercury's intrinsic magnetic field, the MHD (magnetohydrodynamics) and Maxwell's equations are solved as an initial and boundary value problem. In the simulation, the time evolution of the plasma density $\rho$, the bulk velocity $\mathbf{v}$, the pressure $P$, and the magnetic field $\mathbf{B}$ are solved in the Cartesian solar-magnetospheric coordinate system for Mercury with the modified leap-frog method.

The normalized basic MHD and Maxwell's equations and the three-dimensional MHD model were described in detail by *Ogino* [1986] and *Ogino et al.* [1992]. In this study, we concentrated on the southward IMF cases, and we used symmetric mirror boundary conditions against both the noon-midnight meridian and the equatorial planes by solving only a quarter of the real space ($y \leq 0$ and $z \geq 0$). The number of the grid points is (nx, ny, nz) = (600, 158, 158) except for the boundary planes and the grid spacing is uniform by 0.06 $R_M$ in the three directions. Therefore, the simulation domain is $-6.0 \leq x < 30.0$ $R_M$, $-9.5 < y \leq 0.0$ $R_M$, and $0.0 \leq z < 9.5$ $R_M$, and Mercury is set at the origin.

[8] We adopted a static ionospheric solution proposed by *Ogino* [1986] as the inner boundary condition to simulate the low conductivity ("lc") situation near the planetary surface. Namely, the internal quantity $f_{in}$ at the initial state and the external quantity $f_{ex}$ are connected at each time step by introducing a smooth function $\alpha = a_o h/(a_o h + 1)$ as follows:

$$f = \alpha f_{ex} + (1 - \alpha) f_{in} \tag{1}$$

where $f$ represents the physical quantities such as density, bulk velocity, pressure, and magnetic field, which are solved in the MHD simulation. The values $a_o = 30$, $r_a = 0.7R_M$, and $h = (r/r_a)^2 - 1$ for $r > r_a$ and $h = 0$ for $r < r_a$ were used. Because the boundary condition connects the external values to the initial inner values mainly inside the planet, it has little effect on the time evolution of the magnetospheric convection outside the planet. Thus, the boundary condition corresponds to the "lc" case where the surface condition only has a passive effect on the magnetospheric dynamics.

[9] In order to simulate a high conductivity ("hc") case, we added a strong collision term inside the planet to the equation of motion as follows:

$$\frac{\partial \mathbf{v}}{\partial t} = -(\mathbf{v} \cdot \nabla)\mathbf{v} - \frac{\nabla P}{\rho} + \frac{\mathbf{J} \times \mathbf{B}}{\rho} + \mathbf{g} + \frac{\mu \nabla^2 \mathbf{v}}{\rho} - \nu \mathbf{v}, \tag{2}$$

where we used the ion collision frequency $\nu = 3 \times 10^{11}$ $s^{-1}$ to mimic the strong interaction. This value corresponds to $10^{20}$ 1/cc atmosphere density $\times 3 \times 10^{-9}$. Because of the large density, the velocity inside the planet becomes approximately zero. The addition of the collision term tends to tie the foot of each magnetic field line to the planetary surface, which mimics the active effects of the surface condition in the "hc" case.

### 2.2. Three Cases of Global MHD Simulation Results

[10] We used the following solar wind conditions as the input to the global MHD simulation of Mercury's magnetosphere: $\rho$=35 $cm^{-3}$, $\mathbf{v}$ = (–400, 0, 0) km $s^{-1}$, and $\mathbf{B}$ = (0, 0, $Bz_{sw}$). For Case 1, we chose $Bz_{sw}$ = –30 nT for the IMF condition and the "lc" (low conductivity) condition for the internal boundary condition to compare the results with the previous study by *Delcourt et al.* [2003], which used an analytical magnetic and electric field model that rescaled the Earth's magnetosphere under similar conditions. Hereafter, we referred to the rescaled analytical model as the "reference analytical model". In Case 2, we reduced the strength of the southward IMF to $Bz_{sw}$ = –5 nT, and the same "lc" condition was used for the internal boundary condition. Case 3 has the same solar wind conditions as Case 2, and the "hc" (high conductivity) condition is used for the internal boundary.

[11] Figure 1 shows the results of the three MHD simulation cases after quasi-steady states were reached. A remarkable feature is the formation of the near-Mercury neutral line (NMNL) in both Cases 1 and 2 with the "lc" condition. The location of the NMNL is approximately 1.7 (2.1) $R_M$ for Case 1 (2), which is clearly identified with the flow reversal in the equatorial planes (shown with the change from the brown color to the light blue color in Figures 1b and 1d.) The NMNL becomes closer to Mercury when the southward IMF increases from 5 to 30 nT in strength due to the enhanced meridional magnetic convection. The location of the subsolar magnetopause also approaches Mercury from ~1.7 to 1.4 $R_M$ with increasing $|Bz_{sw}|$ because of the strong erosion by the dayside reconnection.

[12] Meanwhile, the location of the flow reversal in the equatorial plane shown in Figure 1f for the "hc" Case 3 is further downtail at approximately X~5 $R_M$ instead of 2.1 $R_M$ in the "lc" Case 2. In the "hc" case, the meridional convection is suppressed due to the strong interaction with the planetary surface, the solar wind-Mercury interaction becomes more viscous-like, and the convection generated at the flanks of the magnetosphere becomes more important. An interesting resultant feature is the enlargement of the stagnant flow region around the planet (the green or yellow area shown in Figure 1f). It should be noted that the tendency of the suppressed convection is the same for the "hc" case with the IMF $Bz_{sw}$ = –30 nT (not shown).

[13] The reference analytical model and the NMNL formation result in different fates of planetary ions. The black line in each panel of Figure 1 shows an example of the $Na^+$ trajectory, which is launched near the vicinity of the planetary surface at 89° of latitude in the noon meridian with an initial energy of 1 eV. None of the test $Na^+$ ions shown in Figure 1 return to Mercury's surface. However, it was confirmed that the $Na^+$ ion with the same initial condition ultimately impacted the planetary surface and consisted of the energetic $Na^+$ precipitation region at the nightside mid-latitudes reported by *Delcourt et al.* [2003] in the reference analytical model. The test $Na^+$ ion in MHD fields first encounters the equatorial plasma sheet at the tailward distance of ~3.0, 2.5, and 10 $R_M$ from Mercury for Cases 1, 2, and 3, respectively. The location corresponds to the sunward flow region in the reference analytical model assuming the DNL (distant neutral line), while it corresponds to the tailward flow regions in the MHD cases due to the NMNL formation. The ion transport in Cases 1 and 2 is similar to that in the reference analytical model until it first encounters the plasma sheet, i.e., the ion is transported from the high-latitude dayside sector into the near-tail in a few minutes. However, once it encounters the plasma sheet at the position tailward of the NMNL, the accelerated $Na^+$ ion experiences a Z-oscillation about the midplane as it travels tailward, and it does not return to the planetary surface regardless of its minimum $\kappa$ parameter during each plasma sheet crossing.

## 3. Systematic Trajectory Tracings of $Na^+$ Ions in MHD Fields

### 3.1. Initial Conditions and Method of Trajectory Tracing

[14] To investigate the dynamics of planetary $Na^+$ ions in Mercury's magnetosphere, we conducted systematic

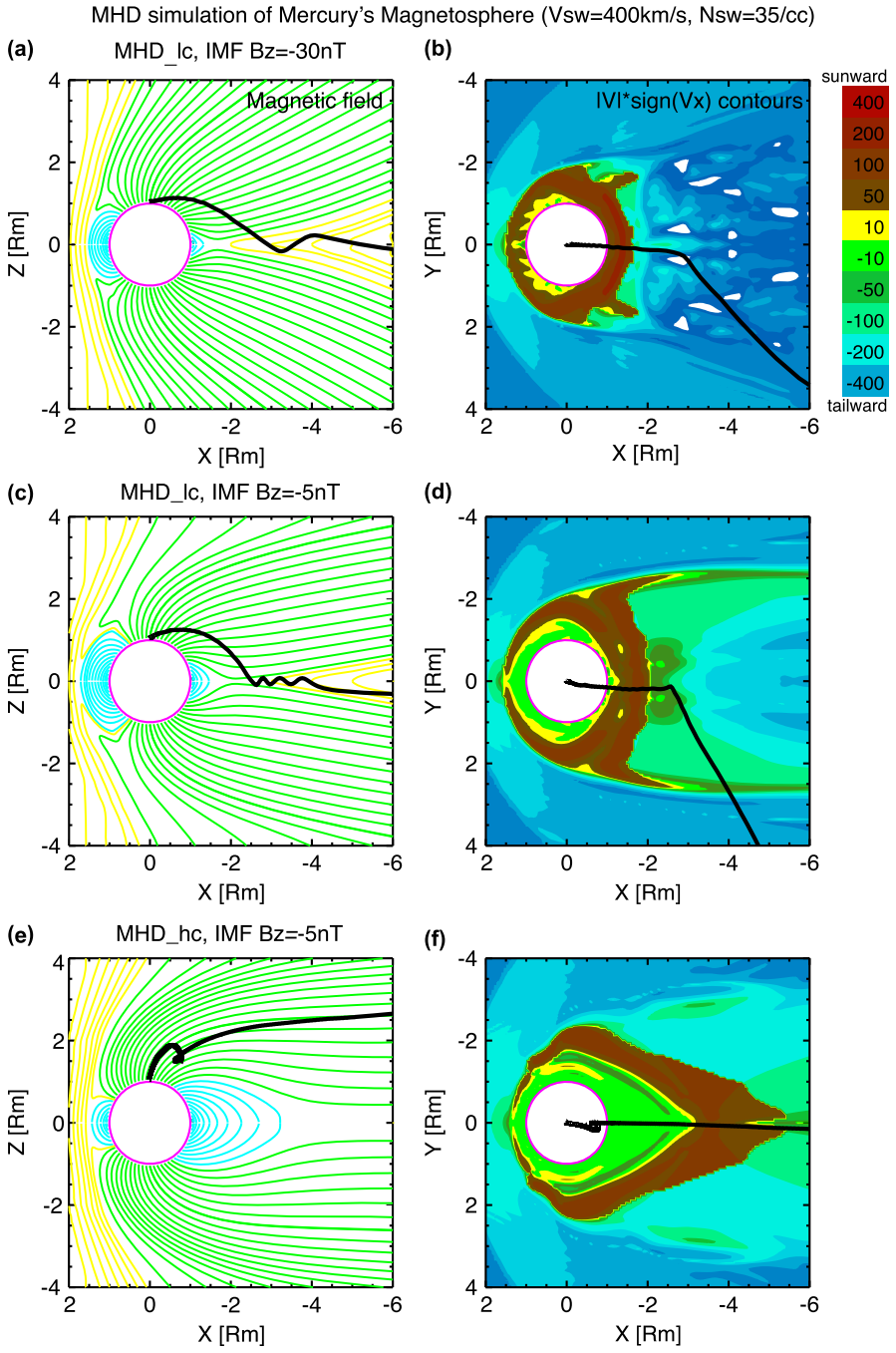


**Figure 1.** (Panels (a), (c), and (e)) The magnetic field configuration in the noon-midnight meridian plane and ((b), (d), and (f)) the distribution of the flow strength in the equatorial plane for three cases of global magnetohydrodynamics (MHD) simulation of Mercury's magnetosphere, which were described in the text. Figures 1a and 1b correspond to Case 1, while Figures 1c and 1d and Figures 1e and 1f show the results for Cases 2 and 3, respectively. The magenta circle in each panel shows the planetary surface. In the left panels, the magnetic field lines are shown in colors: the blue, green, and yellow lines display the closed, open, and detached field lines, respectively. In the right panels, the color contour shows the strength of the flow velocity, which is separated by the sign of Vx, i.e., the light blue (yellow and brown) colors correspond to the tailward (sunward) flow region. The black lines in each panel displays the example of test $Na^+$ trajectory traced in the obtained MHD magnetic and electric field configuration, which was launched from 89° of latitude in the noon meridian near the planetary surface with an initial energy of 1 eV.

trajectory tracings of test $Na^+$ ions in the magnetic and electric configuration obtained from the three cases of the global MHD simulations described in Section 2. Steady MHD fields after the simulation reached the quasi-steady state were used. In order to conserve the magnetic moment by satisfying the solenoidal condition of magnetic field ($div\mathbf{B} = 0$), the cubic spline interpolation method, which ensures to exactly satisfy the solenoidal condition [*Shimizu and Ugai*, 1995], was used to obtain the magnetic field in an arbitrary location in the simulation domain. The electric field ($\mathbf{E}$) was interpolated to satisfy $\mathbf{E} = \mathbf{B} \times \mathbf{v}$ locally.

[15] For the initial condition of the systematic trajectory tracings, the results of a three-dimensional Monte Carlo simulation of Mercury's exosphere at the perihelion were used. The detailed description of the exospheric model can be found in *Leblanc and Johnson* [2003]. The model includes thermal desorption, photon stimulated desorption, micrometeoroid vaporization, and solar wind sputtering in the open field line regions to eject Na from the planetary surface. The direct production of $Na^+$ ions from the surface, such as the electron-stimulated desorption and solar-wind sputtering, was not included in this study. Figure 2 shows the Na density (Figures 2a and 2b) and energy (Figures 2c and 2d) distributions in the exosphere model, which was used as the source of $Na^+$ ions in this study. The density of neutral Na is on the order of $10^3$ [$cm^{-3}$] near the planet, and the initial energy of sodium ions ranges up to ~130 eV.

[16] The method to calculate the moments of $Na^+$ ions in each cubic bin with a volume of $\Delta x^3 = 0.1^3 R_M^3$ is the same as that used in *Delcourt et al.*, [2003]. The magnetospheric circulation of $Na^+$ ions produced via ionization of exospheric neutrals was investigated by attributing a test particle to each bin in Figure 2. We obtained the initial velocities for the test $Na^+$ particles from the exosphere model. Namely, the initial pitch angles and the energies of the test particles were those obtained from Monte Carlo simulations. The flow rate $F_i$ in ions $s^{-1}$ attributed to a test particle associated with a given bin labeled $i$ was also calculated based on the exosphere model as $F_i = \alpha N_i V_i$, where $\alpha$, $N_i$, and $V_i$ are the ionization frequency, the bin density, and the bin volume, respectively. We adopted a typical value of $\alpha$ for the perihelion except for the shadow region in the nightside, where $\alpha$ was set to zero. All test $Na^+$ particles with $\alpha \neq 0$ were traced in the electric and magnetic field models obtained for three cases of the global MHD simulations of Mercury's magnetosphere, which was described in Section 2. The trajectory information was saved in each time that moved to a new magnetospheric grid featuring cubic bins of $0.1R_M$ edge. Integrating the information for all the trajectory passed through each bin, the plasma parameters such as density and characteristic energy in a given bin were calculated.

### 3.2. $Na^+$ Density and Energy Distributions

[17] Figure 3 shows the results of the $Na^+$ density (left panels) and energy (right) obtained for Case 1 shown in Section 2, i.e., under the IMF with $Bz_{sw} = -30$ nT and

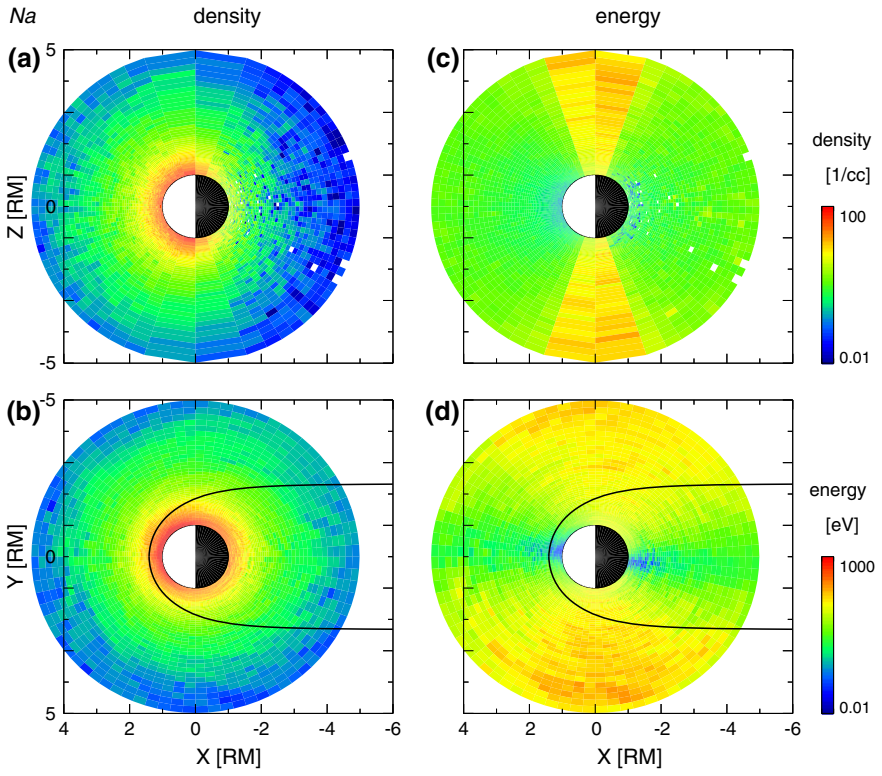


**Figure 2.** The exospheric model at Mercury's perihelion used as the source of $Na^+$ ions in the systematic trajectory tracings. (Panels (a) and (b)) Neutral sodium density and ((c) and (d)) energy are shown with color codes in (top panels) the noon-midnight meridian plane and in (bottom panels) the equatorial plane. The black lines in the bottom panels show the magnetopause location for the reference analytical model [*Delcourt et al.*, 2003].

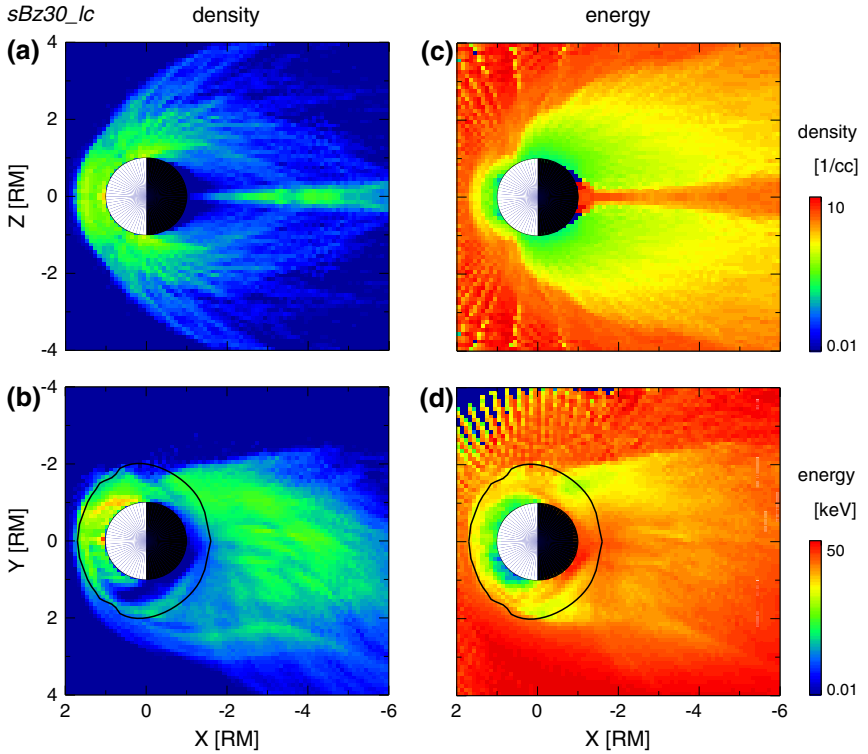


**Figure 3.** The results of systematic trajectory tracings for Case 1, where the interplanetary magnetic field (IMF) condition is Bz = –30 nT and the low conductivity surface condition is used (see Section 2 for details). The (panels (a) and (b)) $Na^+$ density and ((c) and (d)) energy are color-coded according to the color scales shown at the right in the (top panels) noon-midnight meridian plane and in the (bottom panels) equatorial plane. The black lines in the bottom panels show the open closed boundary determined by the Bz direction change in the equatorial plane for the MHD magnetosphere that we used.

"lc" (low conductivity) conditions. In this figure and the following figures, the computational results are presented in both the noon-midnight meridian plane (top panels) and the equatorial plane (bottom panels). Compared with the results from the reference analytical model for the perihelion case (Figures 4 and 7 of *Delcourt et al.* [2003]), in which the solar wind conditions similar to those in Case 1 were assumed, the overall density profile obtained for Case 1 is similar to that obtained using the analytical fields.

[18] Nonetheless, we recognized two different features. One is the lower $Na^+$ density in the inner most part of the plasma sheet. The NMNL formation results in the tailward removal of most $Na^+$ ions. The other feature is the location of the transition region from the dipole-like to the tail-like field configuration in the magnetotail, i.e., the location is much closer for the MHD models, and it roughly corresponds to the open-closed boundary of the magnetic field shown in black lines in the bottom panels of Figure 3. In the nightside region, the boundary corresponds to the location of the NMNL. As reported in the next subsection, the second difference causes the disappearance of the $Na^+$ precipitation band at approximately 30° of latitude, which was reported by *Delcourt et al.* [2003].

[19] When the southward IMF magnitude (sBz) was reduced from 30 nT (Figure 3) to 5 nT (Figure 4), the absence of $Na^+$ ions in the inner most part of the plasma sheet became less apparent. As shown in Section 2, the location of NMNL moves tailward with decreasing magnitude of the southward IMF (sBz). This movement enables more ions to precipitate into the planetary surface, and the density and energy profiles become more similar to the reference analytical model. Another interesting feature is the dense $Na^+$ region in the dayside magnetosphere. This region corresponds to the slow-convection-flow region shown in Figure 1d, and the $Na^+$ ions gradually accelerated to a moderate energy level (typically a few hundreds of eV) because the slow magnetospheric convection is trapped in the closed-field-line region.

[20] The distribution of $Na^+$ ions drastically changed when we used the high conductivity ("hc") planetary surface condition as shown in Figure 5. The warm dense $Na^+$ ion region is extended to the nightside region, as the stagnant slow convection region is extended as shown in Figure 1. The plasma sheet becomes much thicker in the "hc" case than in the "lc" case, and the $Na^+$ energy in the plasma sheet becomes lower in the "hc" case. In the polar region, the suppressed magnetospheric convection, which occurs due to the line-tying effects under a very high-conductivity planetary surface condition, causes cold dense $Na^+$ ions to extend to high altitudes. The cold dense $Na^+$ region on the open field lines at high latitudes and the warm dense $Na^+$ region on the closed field lines at low latitudes are separated by the acceleration region, which is extended from the tail reconnection region at approximately X∼5 $R_M$ (Figure 1f).

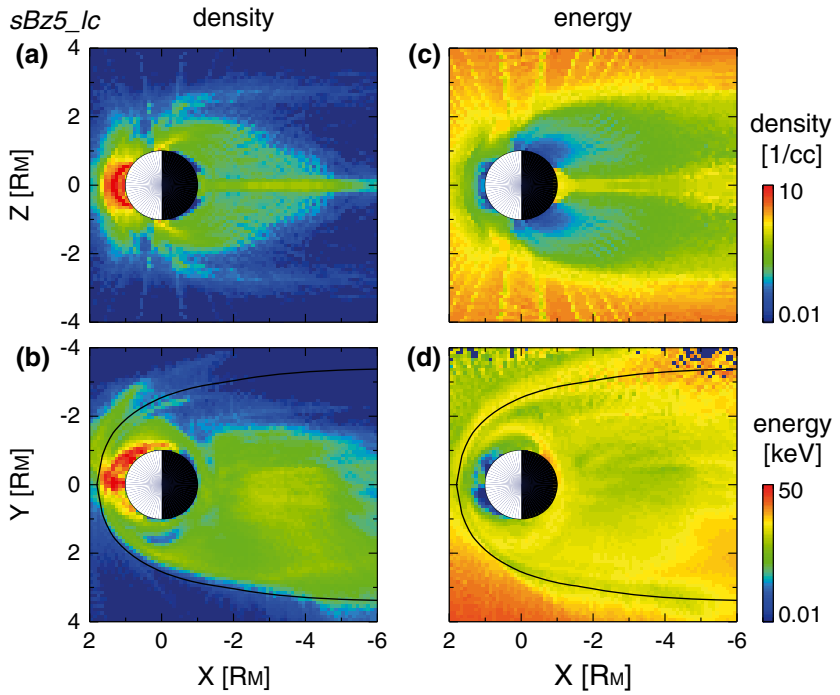


**Figure 4.** The results of systematic trajectory tracings for Case 2, where the IMF condition is Bz = –5 nT and the low conductivity surface condition is used (see Section 2 for details). The format of the figure is the same as that in Figure 3.

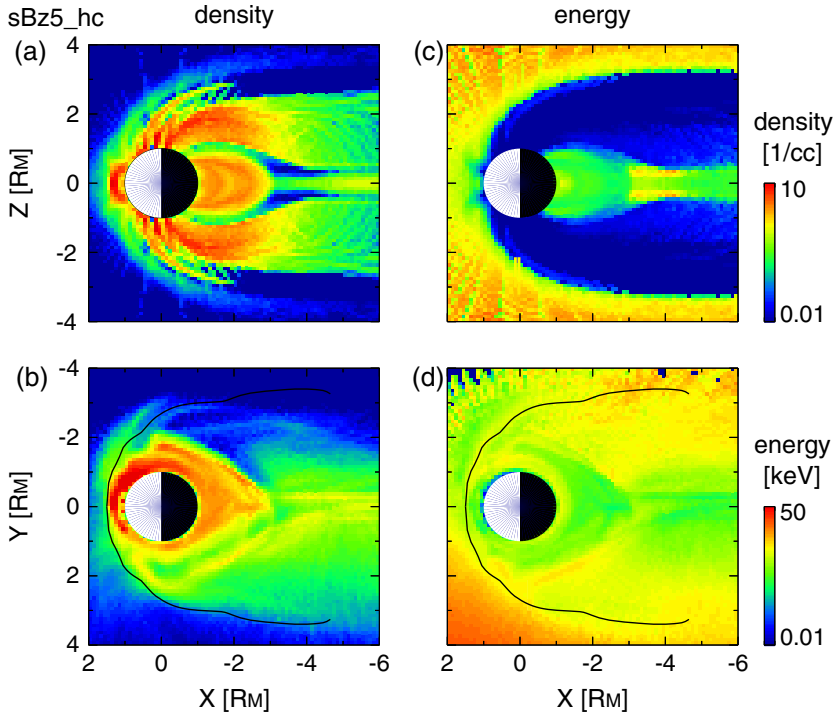


**Figure 5.** The results of systematic trajectory tracings for Case 3, where the IMF condition is Bz= –5 nT and the high conductivity surface condition is used (see Section 2 for details). The format of the figure is the same as that in Figure 3.

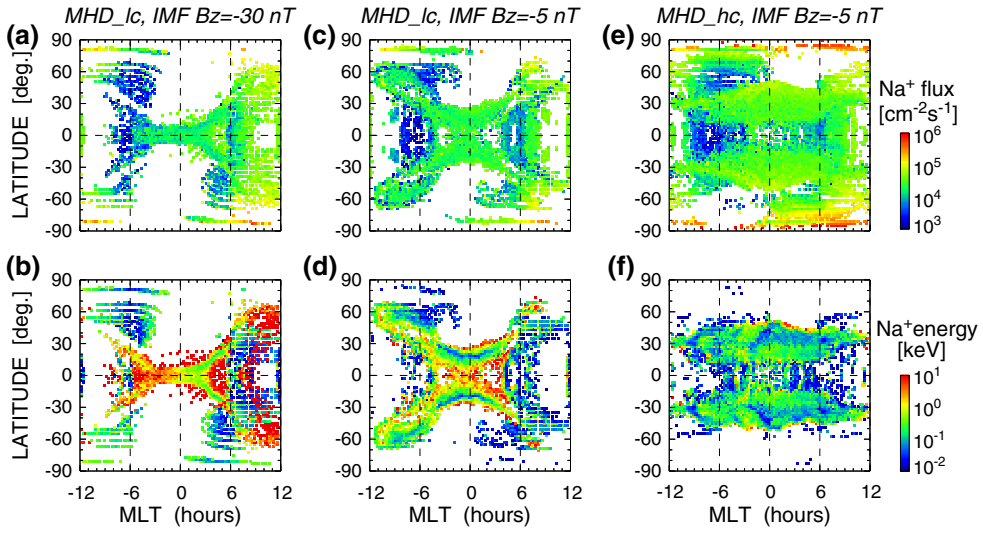


**Figure 6.** Characteristics of precipitating $Na^+$ ions onto Mercury's surface for three cases of the MHD models: (Panels (a) and (b)) Case 1, ((c) and (d)) Case 2, and ((e) and (f)) Case 3. The top and bottom panels show the color-coded ion flux and average energy, respectively. The values outside the color-coded range on the right hand side are displayed with white.

### 3.3. Precipitation Pattern of $Na^+$ Ions Onto Mercury'S Surface

[21] In this subsection, we compared the precipitation patterns of $Na^+$ ions onto the planetary surface between different field models, including the reference analytical model. Figure 6 shows the color-coded $Na^+$ flux and the average energy at impact onto the planetary surface as a function of both longitude and latitude for the three cases of MHD field models described in Section 2. The format of the figure is the same as that in Figure 8 of *Delcourt et al.* [2003]. The previous study with the reference analytical model that assumed the DNL (distant neutral line) showed two $Na^+$ precipitation bands at mid-latitudes (approximately 30°–40° of latitude). However, Figures 6a and 6b show that the result of Case 1, which used the same solar wind condition as the reference model, has no precipitation at the mid-latitude in the nightside. Instead, there are strong precipitations of high-energy $Na^+$ ions around the equatorial region in Case 1, where the $Na^+$ energy becomes higher in the duskside than in the dawnside. The precipitation around the equator and the disappearance of mid-latitude precipitation bands are caused by the NMNL formation, which disconnects the mid-tail and the distant tail from the planetary surface in the MHD simulation.

[22] When we reduced the southward IMF magnitude to 5 nT, the precipitation bands appeared at mid-latitudes in addition to the equatorial high-energy $Na^+$ precipitation region as shown in Figures 6c and 6d, because the NMNL moves tailward with decreasing southward IMF magnitude, the finite $\kappa$ effects noted by *Delcourt et al.* [2003] becomes visible in Case 2. However, the high-latitude boundary of the mid-latitude precipitation bands in the nightside is limited by the location of the NMNL, and this boundary is lower than that for the reference analytical model ($\sim$ 40°).

[23] In the case of high conductivity ("hc") surface condition (Case 3) shown in Figures 6e and 6f, precipitation of moderate-energy $Na^+$ ions are observed up to the $\sim$ 50° of latitude. This precipitation corresponds to the warm dense $Na^+$ ions trapped in the slow-convection region at low latitudes reported in the previous subsection.

[24] Recent MESSENGER observations revealed that the $Na^+$ fluxes peak near the magnetic-cusp regions and the magnetotail region especially in the dusk side [*Zurbuchen et al.*, 2011]. Enhancement of the flux in the magnetotail and the dawn-dusk asymmetry is consistent with the results of trajectory tracings in the "lc" cases. The cusp moves to lower latitude in the "hc" case at $\sim$ 30–4°0, and the location of the flux enhancement in the cusp observed by MESSENGER seems more consistent with the "lc" cases. However, the global distribution can change with the effects of IMF $B_x$ and $B_y$, and the direct comparison with observations is beyond the scope of this study.

## 4. Summary and Discussion

[25] Systematic trajectory tracings of $Na^+$ ions in three cases of MHD fields were performed. Case 1 is under similar solar wind conditions to the reference analytical model used in *Delcourt et al.* [2003] with IMF $B_z$ = –30 nT and a low conductivity ("lc") planetary surface at the inner boundary. Case 2 corresponds to a smaller IMF magnitude of $B_z$ = –5 nT and the same setting for other conditions with "lc". Case 3 has the same solar wind conditions as Case 2 and a high conductivity ("hc") planetary surface condition. For systematic trajectory tracings, the initial conditions of each particle were taken from a simplified exospheric Na model derived from [*Leblanc and Johnson*, 2003]. The results are summarized as follows:

[26] 1. The density profile obtained for MHD with the low conductivity (lc) boundary at the planetary surface is similar to that obtained with the reference analytical field model.

[27] 2. The $Na^+$ precipitation band at approximately 30° of latitude in the reference analytical model disappeared in

the "lc" MHD case due to the near-Mercury neutral line (NMNL) formation in the magnetotail.

[28] 3. The change in the $Na^+$ band depends on the strength of the southward IMF (sBz). In the sBz 5 case, the $Na^+$ band is formed at latitudes of < 30°.

[29] 4. In the weak IMF (sBz 5) case, the dense $Na^+$ region is formed in the dayside magnetosphere, where warm $Na^+$ ions of approximately a few hundred eVs are trapped.

[30] 5. In the "hc" MHD case, the magnetospheric convection through the polar regions is suppressed, which results in regions of warm dense $Na^+$ at low latitudes and cold dense $Na^+$ at high latitudes.

[31] Recent magnetic field observations by MESSENGER showed a best-fit planetary dipole moment of 195 T$\pm$10 nT-$R_M^3$ with an offset of 484$\pm$11 km northward of the geographic equator [*Anderson et al.*, 2011]. The present study did not consider the offset dipole to make a close comparison with the previous study that used the reference analytical model [*Delcourt et al.*, 2003]. A recent study using statistical trajectory tracings in an analytical model with an offset dipole [*Delcourt et al.*, 2012] showed that the inclusion of the offset does not change qualitative properties of the $Na^+$ distribution. The qualitative features obtained from comparing different field models, such as the effects of the NMNL and the surface conductivity, were expected to be similar, while the offset will cause the asymmetry of the precipitation patterns between the northern and southern hemispheres. The large solar wind aberration is also a possible cause of additional asymmetry of the precipitation patterns.

[32] The results indicate that the appearance of mid-latitude precipitation bands drastically changes with the existence and the location of the NMNL. In the Earth's magnetosphere, the near-Earth neutral line is often formed in association with substorms [e.g., *Nishida et al.*, 1996; *Baumjohann et al.*, 1999] . Thus, the precipitation pattern of $Na^+$ ions onto Mercury's surface may change significantly with the activity level of Mercury's magnetosphere. The results also show that the warm dense $Na^+$ population can exist in the inner Mercury's magnetosphere in a small southward IMF case. The formation mechanism is similar to that proposed for the "sodium ring current" by *Yagi et al.* [2010] with the low solar wind dynamic pressure condition. Our result also shows that the warm dense $Na^+$ region can be more extended to the nightside region if the surface conductivity is high. Therefore, we can learn about the surface conductivity by observing the magnetospheric convection, the distribution of $Na^+$ ions around the planet, or the precipitation pattern of $Na^+$ ions onto the planetary surface.

[33] **Acknowledgments.** This work is supported by the Research Grant of the Toyoaki Shogakukai and the Type-II Research Grant of the Institute for Advanced Research, Nagoya University.

## References

Anderson, B. J., M. H. Acuna, H. Korth, M. E. Purucker, C. L. Johnson, J. A. Slavin, S. C. Solomon, and R. L. McNutt Jr (2008), The structure of Mercury's magnetic field from MESSENGER's first flyby, *Science*, *321*, 82–85 , doi:10.1126/science.1159081.

Anderson, B. J., C. L. Johnson, H. Korth, M. E. Purucker, R. M. Winslow, J. A. Slavin, S. C. Solomon, R. L. McNutt Jr, J. M. Raines, and T. H. Zurbuchen (2011), The global magnetic field of Mercury from MESSENGER orbital observations, *Science*, *333*, 1859–1862.

Baumjohann, W., M. Hesse, S. Kokubun, T. Mukai, T. Nagai, and A. A. Petrukovich (1999), Substorm dipolarization and recovery, *J. Geophys. Res.*, *104*, 24995–25000.

Bida, T. A., R. M. Killen, and T. H. Morgan (2000), Discovery of calcium in Mercury's atmosphere, *Nature*, *404*, 159–161.

Broadfoot, A. L., D. E. Shemansky, and S. Kumar (1976), Mariner 10: Mercury atmosphere, *Geophys. Res. Lett.*, *3*, 577–580.

Delcourt, D. C., S. Grimald, F. Leblanc, J.-J. Berthelier, A. Millilo, A. Mura, S. Orsini, and T. E. Moore (2003), A quantitative model of the planetary $Na^+$ contribution to Mercury's magnetosphere, *Ann. Geophys.*, *21*, 1723–1736.

Delcourt, D. C., and K. Seki (2006), On the dynamics of charged particles in the magnetosphere of Mercury, *Adv. Geosci.*, W.-H. Ip and A Bhardwaj Eds, *3*, 17–28, doi:10.1142/9789812707192_0003.

Delcourt, D. C., K. Seki, N. Terada, and Y. Miyoshi (2005), Electron dynamics during substorm dipolarization in Mercury's magnetosphere, *Ann. Geophys.*, *23*, 3389–3398.

Delcourt, D. C., K. Seki, N. Terada, and T. Moore (2012), Centrifugally stimulated exospheric ion escape at Mercury, *Geophys. Res. Lett.*, *39*, L22105, doi:10.1029/2012GL054085.

Fujimoto, M., W. Baumjohann, K. Kabin, R. Nakamura, J. A. Slavin, N. Terada, and L. Zelenyi (2007), Hermean Magnetosphere-Solar Wind Interaction, *Space Sci. Rev.*, *132*, 529–550, doi:10.1007/s11214-007-9245-8.

Janhunen, P., and E. Kallio (2004), Surface conductivity of Mercury provides current closure and may affect magnetospheric symmetry, *Ann. Geophys.*, *22*, 1829–1837.

Kabin, K., and T. I. Gombosi (2000), Interaction of Mercury with the solar wind, *Icarus*, *84*, 397–406.

Kallio, E., and J. P. Janhunen (2004), The response of the Hermean magnetosphere to the interplanetary magnetic field, *Adv. Spa. Res.*, *33*, 2176–2181, doi:10.1016/S0273-1177(03)00447-2.

Kameda, S., I. Yoshikawa, J. Ono, and H. Nozawa (2007), Time variation in exospheric sodium density on Mercury, *Planet. Space Sci.*, *55*, 1509–1517, doi:10.1016/j.pss.2006.10.010.

Leblanc, F., and R. E. Johnson (2003), Mercury's sodium exosphere, *Icarus*, *164*, 261–281, doi:10.1016/S0019-1035(03)00147-7.

Luhmann, J. G., C. T. Russell, and N. A. Tsyganenko (1998), Disturbances in Mercury's magnetosphere: Are the Mariner 10 "substorms" simply driven, *J. Geophys. Res.*, *103*, 9113–9119.

McClintock, W. E., E. T. Bradley, R. J. Vervack Jr., R. M. Killen, A. L. Sprague, N. R. Izenberg, and S. C. Solomon (2008), Mercury's exosphere: Observations during MESSENGER's first Mercury flyby, *Science*, *321*, 92–94.

Mura, A., A. Milillo, S. Orsini, and S. Massetti (2007), Numerical and analytical model of Mercury's exosphere: Dependence on surface and external conditions, *Planet. Space Sci.*, *55*, 1569–1583, doi: 10.1016/j.pss.2006.11.028.

Ness, N. F., K. W. Behannon, R. P. Lepping, and Y. C. Whang (1975), Macnetic field of Mercury 1, *J. Geophys. Res.*, *80*, 2708–2716.

Nishida, A., T. Mukai, T. Yamamoto, Y. Saito, and S. Kokubun (1996), Magnetotail convection in geomagnetically active times 1. Distance to the neutral lines, *J. Geomag. Geoelectr.*, *48*(5-6), 489–501.

Ogilvie, K. W., J. D. Scudder, V. M. Vasyliunas, R. E. Hartle, and G. L. Siscoe (1977), Observations at planet Mercury by plasma electron experiment: Mariner 10, *J. Geophys. Res.*, *82*, 1807–1824.

Ogino, T. (1986), A three-dimensional MHD simulation of the interaction of the solar wind with the Earth's magnetosphere: The generation of field-aligned currents, *J. Geophys. Res.*, *91*, 6791–6806.

Ogino, T., R. J. Walker, and M. Ashour-Abdalla (1992), A global magnetohydrodynamic simulation of the magnetosheath and magnetopause when the interplanetary magnetic field is northward, *IEEE Trans. Plasma. Sci.*, *20*, 817–828.

Potter, A. E., and T. H. Morgan (1985), Discovery of sodium in the atmosphere of Mercury, *Science*, *229*, 651–653.

Potter, A. E., and T. H. Morgan (1986), Potassium in the atmosphere of Mercury, *Icarus*, *67*, 336–340.

Sarantos, M., J. A. Slavin, M. Benna, S. A. Boardsen, R. M. Killen, D. Schriver, and P. Travncek (2009), Sodium-ion pickup observed above the magnetopause during MESSENGER's first Mercury flyby: Constraints on neutral exospheric models, *Geophys. Res. Lett.*, *36*, L04106, doi: 10.1029/2008GL036207.

Siscoe, G. L., N. F. Ness, and C. M. Yeates (1975), Substorms on Mercury? *J. Geophys. Res.*, *80*, 4359–4363.

Slavin, J. A., et al. (2008), Mercury's magnetosphere after MESSENGER's first flyby, *Science*, *321*, 85–89, doi:10.1126/science.1159040.

Slavin, J. A., et al. (2009), MESSENGER observations of Mercury's magnetosphere during northward IMF, *Geophys. Res. Lett.*, *36*, L02101, doi:10.1029/2008GL036158.

Slavin, J. A., et al. (2010), MESSENGER observations of extreme loading and unloading of mercury's magnetic tail, *Science*, *329*, 665, doi:10.1126/science.1188067.

Slavin, J. A., et al. (2012), MESSENGER and Mariner 10 flyby observations of magnetotailăstructure and dynamics at Mercury, *J. Geophys. Res.*, *117*, A01215, doi:10.1029/2011JA016900.

Shimizu, T., and M. Ugai (1995), Computational method of particle trajectories for conserving adiabatic invariants in discrete electro-magnetic fields, *J. Jpn. Soc. Ind. Appl. Math.*, *5*(4), 423–444.

Yagi, M., K. Seki, Y. Matsumoto, D. C. Delcourt, and F. Leblanc (2010), Formation of a sodium ring in Mercury's magnetosphere, *J. Geophys. Res.*, *115*, A10253, doi:10.1029/2009JA015226.

Zurbuchen, T. H., J. M. Raines, G. Gloeckler, S. M. Krimigis, J. A. Slavin, P. L. Koehn, R. M. Killen, A. L. Sprague, R. L. McNutt Jr., and S. C. Solomon (2008), MESSENGER observations of the compositions of Mercury's ionized exosphere and plasma environment, *Science*, *321*, 90–92, doi:10.1126/science.1159314.

Zurbuchen, T. H., et al. (2011), MESSENGER observations of the spatial distribution of planetary ions near Mercury, *Science*, *333*, 1862–1865, doi:10.1126/science.1211302.